

Multi-scale characterization of spatially heterogeneous systems: implications for discontinuously reinforced metal–matrix composite microstructures

J.E. Spowart^{b,*}, B. Maruyama^a, D.B. Miracle^a

^a AF Research Laboratory, Materials and Manufacturing Directorate, Building 655, 2230 10th Street Suite 1, Wright Patterson AFB, Dayton, OH 45433, USA

^b UES, Dayton, OH 45432, USA

Received 26 September 2000; received in revised form 16 November 2000

Abstract

A new multi-scale technique is presented for characterizing the spatial distribution of second-phase particles in two-dimensional distributed multi-phase systems. The implications for the characterization of reinforcement distributions in discontinuously reinforced metallic matrix composite microstructures are discussed, along with results of the analysis both for simulated and experimental discontinuously reinforced aluminum (DRA) materials. A systematic variation in the degree of spatial heterogeneity is observed with increasing length scale. This result leads to the definition of the parameter L_H or homogeneous length scale. The relevance of L_H measured for a real DRA microstructure is then discussed in the context of statistical variations in mechanical properties such as tensile strength, ductility, and fracture toughness. © 2001 Published by Elsevier Science B.V.

Keywords: Spatial distribution; Homogeneous length scale; Discontinuously reinforced aluminum

1. Introduction

Simple scalar descriptions of microstructures have been quite successful in the previous decades in helping understand and predict material behavior. Models such as Hall-Petch, the ‘rule of mixtures’, Orowan, and creep models such as Harper-dorn, Coble, etc. describe microstructure by simple scalar quantities such as mean grain size, average inter-particle spacing, or volume fraction. Information relating to the spatial distribution or the distribution about the mean quantity is ignored in these models. While these approaches have been very successful in predicting and understanding the behavior of a wide range of materials, there are materials systems and properties, where such models do not perform well. Discontinuously reinforced metallic matrix composites (MMCs) is one such class of materials.

There is in the open literature a wealth of experimental and theoretical evidence suggesting that the uniformity of reinforcement spatial distribution plays a key role in controlling the yield strength [1], ductility [2], fatigue [3] and fracture [4,5] behavior of discontinuously reinforced MMCs. Although the mechanisms which control these properties are still quite poorly understood, and unambiguous evidence of the specific influence of particle distribution has not been obtained, there is general agreement that microstructures with more heterogeneous spatial distributions of reinforcement particles (i.e. ‘clustered’ microstructures) tend to have poorer mechanical properties. However, a large part of the problem in linking microstructural heterogeneity with mechanical properties is that unambiguous definitions of fundamental terms required to quantify spatial distribution, such as ‘homogeneous,’ ‘random,’ and ‘cluster’ are not available. In addition, techniques for characterizing the spatial distribution of reinforcement particles have been slow to develop, and are still somewhat limited in scope. For example, Schwarz and Exner [6] measured nearest-neighbor distances in 2-D

* Corresponding author. Tel.: +1-937-2551340; fax: +1-937-2553007.

E-mail address: jonathan.spowart@afrl.af.mil (J.E. Spowart).

and 3-D, and used this to determine the presence or absence of clustering. In addition, a number of researchers [2,7–12] have used tessellation techniques to divide the microstructure up into space-filling cells, each containing a single reinforcement particle. The statistics of the distribution of cell sizes thus produced were then used to characterize the distribution of particles. The main objection to these techniques is that it necessarily assigns a length scale to the problem, i.e. that of the mean inter-particle spacing, or nearest-neighbor distance. Aspects of the spatial arrangement of particles at length scales above this are ignored. Furthermore, there are practical difficulties associated with image analysis, specifically with the thresholding techniques typically used to define boundaries between the individual reinforcement particles, especially when the particles are very small, poorly contrasted with the matrix, or are highly clustered.

Other researchers [13–15] have concentrated on obtaining information about particle spatial distributions based on the acquisition of multi-point correlation functions. For example, Berryman [15] used image analysis to obtain the 2-point correlation function of a 2-D section through a synthetic 3-D microstructure comprising fully overlapping spheres. The level of agreement between the measured 2-point correlation function and the available closed-form solutions was good, therefore validating the technique. The author goes on to suggest that an interesting problem to tackle would be the extension of the analysis to cover different microstructural length scales. Lu and Torquato [13] demonstrated that the 2-point correlation function could indeed be used to obtain information about local volume fractions on several length scales, however the calculations involved in this approach are quite complex. Work in this area has therefore concentrated mainly on model systems, for which closed-form solutions of the 2-point correlation function exist.

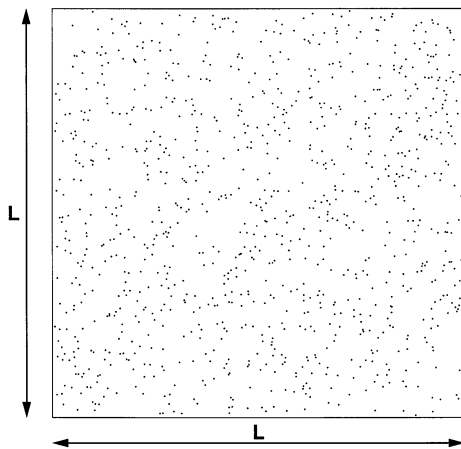


Fig. 1. Ensemble of points placed at random coordinates within a plane of area L^2 . (Number of points, $N = 1000$).

The objective of the current paper is to introduce a more direct approach for characterizing and analyzing 2-D distributed second phases on multiple length scales, using simple image analysis techniques and without obtaining the 2-point correlation function. In addition, a practical definition for homogeneity will be described. The methodology will then be applied to the microstructure of discontinuously reinforced MMCs. With this technique, information on the distribution of particles can be obtained at length scales from the particle diameter up to the specimen size itself. An advantage of this technique is that it can therefore be used to analyze the microstructure at length scales encompassed by many different potential failure mechanisms. Additionally, a single mechanism can be captured operating on multiple length scales. For example, near-threshold fatigue crack growth is typically associated with a small plastic zone size compared to the particle size, whereas fatigue cracks propagating at large ΔK can generate a plastic zone that encompasses many particle diameters [16,17]. The ability to assess the spatial heterogeneity of the microstructure at many different length scales is therefore an invaluable tool in the effort to correlate microstructure with mechanical properties in distributed multi-phase systems such as discontinuously reinforced MMCs.

1.1. Point counting techniques

Statistical techniques based on counting the numbers of points in different sized sub-areas within a large field can be an effective tool for measuring levels of spatial variability in the distribution of points [18–21]. For example, Fig. 1 shows an ensemble of $N = 1000$ points placed at random within an area L^2 . If one divides up the area L^2 into smaller areas (‘quilt squares’) of side length Q , then the statistical variability in the numbers of points counted in each individual quilt square can be used to measure the spatial variability of the whole ensemble. Furthermore, if we assume that the points are placed at coordinates chosen entirely at random within the area L^2 , then the numbers of particles counted in individual quilt squares should follow Poisson¹ statistics [22]. In which case, the individual point counts will follow the distribution function given in Eq. (1).

$$p(n_i) = \frac{n_i^n \exp(-n)}{n_i!}. \quad (1)$$

Here, $p(n_i)$ is the probability of counting n_i points within a quilt square and n is the average number of particles counted in each square, i.e., $n = \sum_i n_i p(n_i)$.

¹ We must also assume that the total number of points counted in any quilt square will be small and will also be independent of the number counted in any other quilt square.

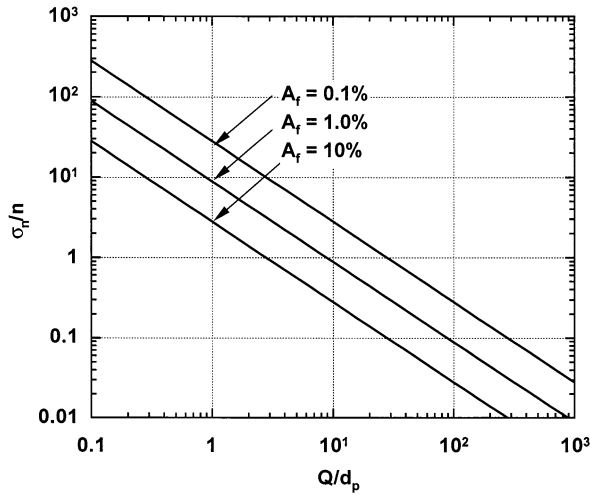


Fig. 2. Plot showing relationship between σ_n/n and Q/d_p for different area fractions (0.1%, 1.0%, 10%), according to Eq. (4).

Obviously, n will scale with the second power of the chosen quilt size, Q , and linearly with the overall number density of points. Additionally, for a Poisson distribution of point counts the following relationship is also true:

$$\sigma_n = \sqrt{n}, \quad (2)$$

where, σ_n is the population standard deviation for individual point count values.

1.2. Particle counting techniques

In order to apply the above treatment to a microstructure containing discrete, non-overlapping particles, we must first take into account the particles' finite size. If we assume that the particles are small and that the area fraction that they cover is low, then their centroid coordinates will be largely uncorrelated and Poisson statistics will still be appropriate. For monosized particles of diameter d_p we can therefore write the following:

$$n = \left(\frac{2Q}{\sqrt{\pi}d_p} \right)^2 A_f, \quad (3)$$

where Q is the length of the quilt square side, and A_f is the area fraction covered by the particle ensemble. By substituting Eq. (3) in Eq. (2), and rearranging, we obtain:

$$\frac{\sigma_n}{n} = \left(\frac{\pi}{4A_f} \right)^{0.5} \left(\frac{Q}{d_p} \right)^{-1}. \quad (4)$$

This relationship is plotted in Fig. 2, for area fractions from 0.1% to 10%.

At any given quilt size, Q , Eq. (3) predicts a linear relationship between n and A_f . Therefore Eq. (4) can also be rewritten in terms of localized area fraction statistics as Eq. (5) below:

$$\frac{\sigma_{A_f}}{A_f} = \left(\frac{\pi}{4A_f} \right)^{0.5} \left(\frac{Q}{d_p} \right)^{-1}. \quad (5)$$

Although Eq. (5) is similar in form to the ‘‘coarseness parameter’’ as derived from the 2-point correlation function by Lu and Torquato [13], additional work will be necessary in order to ascertain whether the two relationships are functionally identical. This work will form the basis of a follow-on paper.

2. Multi-scale analysis of area fractions

The ability to obtain statistical information about the variability of reinforcement particle area fractions over various different length scales forms the basis of a flexible, multi-scale analysis for spatial heterogeneity in distributed multi-phase systems. In order to assess the applicability of the multi-scale analysis of area fraction (MSAAF) technique for characterizing spatial heterogeneity, large numbers of statistically similar microstructures must be analyzed. Rather than relying on the time-consuming technique of obtaining multiple plane sections through actual particle-reinforced microstructures, it was found to be more efficient to simulate individual particle spatial distributions using a series of specially developed computer codes [23–25]. Subtle differences between particle distributions could then be introduced in a controlled manner.

2.1. Construction of synthetic microstructures

The computer code utilized for the production of the synthetic microstructures was able to take a population of 2-D particle sections (disks) and place them, one at a time, at specific X – Y coordinates within an image plane of known size. This resulted in a synthetic microstructure with a predetermined area fraction and number of particles. A random number generator was used to select the coordinates at which a new particle was to be placed. These particle coordinates were rejected if the new particle overlapped with an existing particle, and new coordinates were chosen. The process was repeated until all the particles were placed on the image. Fig. 3 shows an example of a synthetic microstructure produced in this way, containing 1000 monosized particles at an area fraction of 10%.

It is important to realize that the resulting spatial distribution of particle centroids is not *truly* random, as the particles are consistently placed so that they do not overlap. However, this effect only becomes significant at the highest area fractions (Section 2.3).

2.2. Multi-scale analysis of area fraction by digital image re-sampling

The procedure that was developed for characterizing the multi-phase microstructures is best described as a

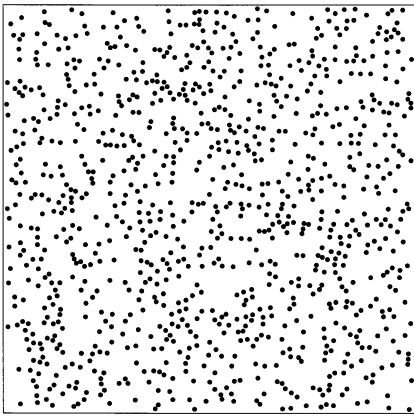


Fig. 3. Synthetic microstructure utilizing random, non-overlapping particle placement (area fraction of particles, $A_f = 10\%$, number of particles, $N = 1000$).

digital image re-sampling technique. Microstructural images that are obtained either from digital microscopy

or by direct computer simulation are re-sampled by replacing groups of adjacent pixels with a single (larger) pixel. The gray level of the new pixel is assigned based on the mean gray level of the pixels being replaced. This process is repeated at successively coarser length scales, simply by decreasing the pixel resolution of the image, as shown in Fig. 4(a)–(d). In this procedure, the statistics of local area fractions are obtained by measuring the gray level in each individual quilt square (i.e. pixel) of the re-sampled image.² Note that although the mean area fraction of each re-sampled image remains constant, the variability in area fraction (pixel values) about the mean decreases with increasing coarseness of the re-sampling, i.e., there is a reduction in image *contrast*, but not in image *brightness* as the pixel resolution is decreased.

Fig. 5 shows how the variability in area fraction (expressed as the coefficient of variation in area fraction, σ_{A_f}/A_f) changes with increasing quilt size, Q . This type of plot is subsequently referred to as an MSAAF

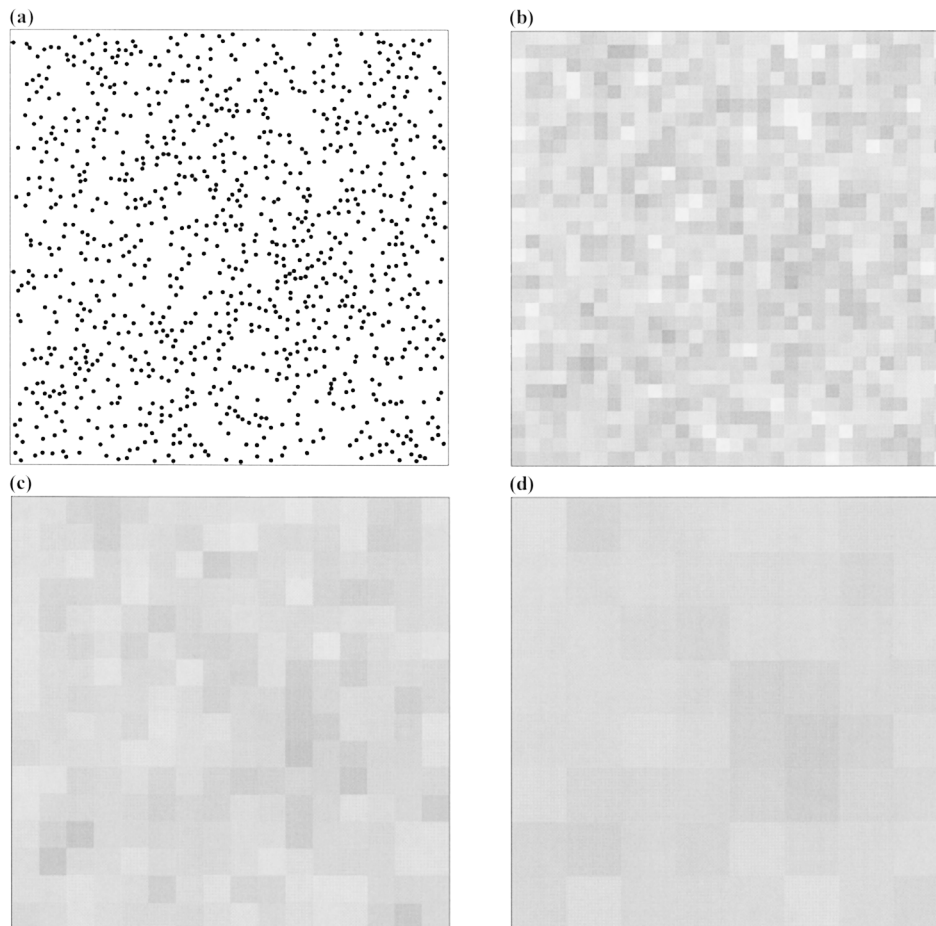


Fig. 4. A series of quilting operations applied to an image containing 1000 particles at an area fraction of 10%. (a) Raw image at a resolution of 1024×1024 pixels, (b) re-sampled at 32×32 pixels, (c) resampled at 16×16 pixels, and (d) resampled at 8×8 pixels.

² For an 8-bit grayscale image, the area fraction within each quilt square is equal to measured gray level/256.

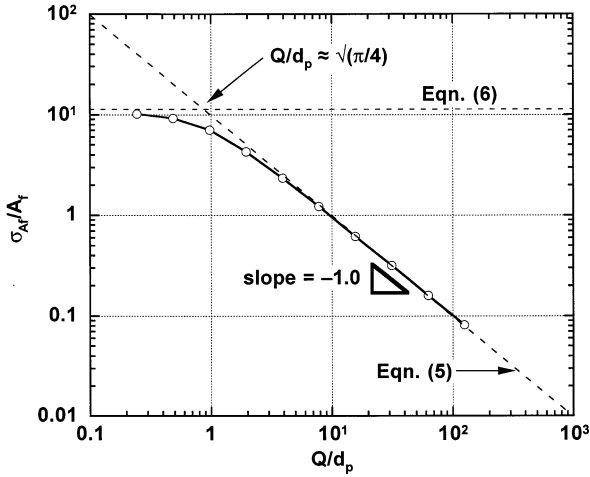


Fig. 5. The non-dimensional variability parameter, σ_{A_f}/A_f plotted vs. the normalized quilt size, Q/d_p . The broken sloping line is the prediction from Eq. (5), assuming Poisson statistics with a vanishing area fraction. Also indicated on the plot is the point corresponding to simultaneous solution of Eq. (5) and Eq. (6), at a quilt size $Q/d_p = Q^*/d_p$. The original image was 4096×4096 pixels. ($A_f = 0.8\%$, $N = 10\,000$).

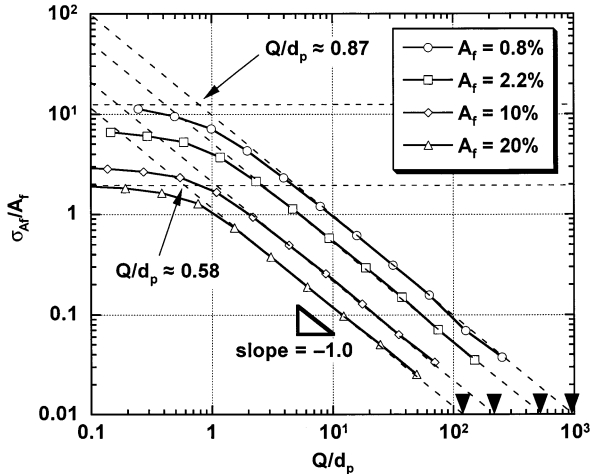


Fig. 6. MSAAF plot, showing effect of increasing area fraction for random, non-overlapping particle distributions. Small arrows on the lower right horizontal axis indicate values of L_H (Section 2.3.1) evaluated at $\sigma_{A_f}/A_f = 0.01$ ($N = 10\,000$).

plot. After an initially horizontal slope, the plotted curve shows good agreement between the measured values of σ_{A_f}/A_f and the relationship predicted by Eq. (5) over several orders of magnitude of quilt size, Q . Note that on this and all subsequent MSAAF plots, Q is normalized with respect to the (mean) particle diameter, d_p .

The upper limit for σ_{A_f}/A_f shown by the broken horizontal line in Fig. 5 can be determined³ from the

³ At small values of Q/d_p , the binary image contains only two populations of pixels (black and white) in proportions A_f and $(1 - A_f)$ respectively. Eq. (6) is therefore obtained by solving the equation, $\sigma_{A_f}^2 = \frac{1}{N} \left(\sum_1^{N A_f} (1 - A_f)^2 + \sum_{N A_f}^N A_f^2 \right)$ for this particular case.

area fraction of the original image, according to Eq. (6):

$$\frac{\sigma_{A_f}}{A_f} \Big|_{Q/d_p \rightarrow 0} = \left(\frac{1 - A_f}{A_f} \right)^{0.5} \quad (6)$$

Additionally, the point of intersection of the two lines given by Eq. (5) and Eq. (6), at a quilt size Q^*/d_p , is given by Eq. (7):

$$\frac{Q^*}{d_p} \left(\frac{1 - A_f}{A_f} \right)^{0.5} = \left(\frac{\pi}{4 A_f} \right)^{0.5} \quad (7)$$

For the case of non-interacting, (i.e. randomly placed) monosized particles at very low volume fractions, Eq. (7) reduces to the following:

$$\frac{Q^*}{d_p} = \left(\frac{\pi}{4(1 - A_f)} \right)^{0.5} \approx \sqrt{\frac{\pi}{4}} \quad (8)$$

The size of Q^*/d_p is important because the start of the linear regime on the MSAAF plot is observed to scale with this parameter. Q^*/d_p therefore effectively defines the length scale below which the MSAAF technique no longer accurately describes the statistics of the reinforcement spatial distribution.

2.3. Influence of area fraction on random, non-overlapping monosized particle distributions

Fig. 6 shows the effect on the MSAAF plot of increasing the area fraction for random, non-overlapping distributions of particles. Each of these microstructures contained 10 000 monosized particles. Although the slopes over the linear portions are all -1.0 , it should be noted that Q^*/d_p decreases quite rapidly from the Poisson prediction (Eq. (8)) as A_f is increased from 0.8% to 20%. This is due to the higher area fraction random microstructures being less ‘Poisson-like’ (i.e. more homogeneous) than the lower area fraction random microstructures, because of the imposed constraint of having non-overlapping particles (Section 2.4.1).

2.3.1. Defining the homogeneous length scale (L_H)

The MSAAF plot can be characterized by measuring the quilt size at which the curve intercepts the lower horizontal axis at a certain value of σ_{A_f}/A_f . This intercept, subsequently referred to as L_H , effectively defines the length scale above which the local variability in area fraction is smaller than the specified σ_{A_f}/A_f . Since reinforcement volume fractions in discontinuously reinforced composite materials are often specified to $\pm 1\%$ or better [26], a value of $\sigma_{A_f}/A_f = 0.01$ has practical relevance. For example, the MSAAF curve shown in Fig. 6 for the random distribution of particles at an area fraction of $A_f = 20\%$ gives $L_H(0.01) \approx 100 d_p$.

Fig. 7 shows how values of $L_H(0.01)/d_p$ measured in these random, non-overlapping microstructures decrease monotonically with increasing area fraction, up to $A_f = 45\%$. Extrapolation of the fitted curve to the horizontal axis at $L_H = 0$ agrees with the theoretical limit for 2-D packing of monosize disks (called the 2-D ‘jamming limit’ [27]) at $A_f \approx 0.547$. As the area fraction approaches the jamming limit, the numbers of different spatial arrangements available to the particles become very limited, thus minimizing possible variations in area fraction.

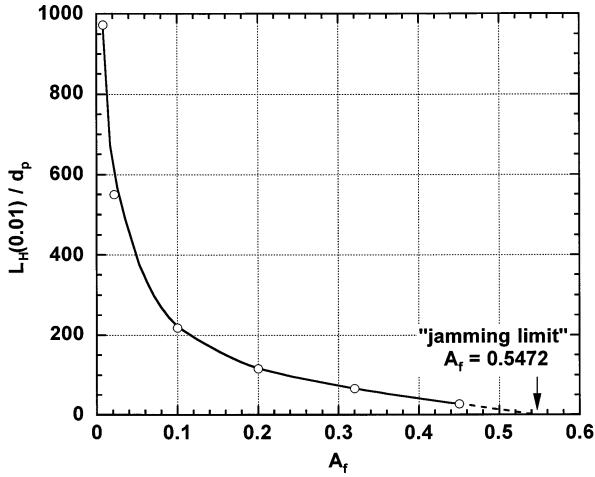


Fig. 7. Effect on L_H of increasing area fraction for random, non-overlapping particle distributions ($N = 10\,000$). Extrapolation of fitted curve agrees with 2-D ‘jamming limit’ for random, non-overlapping circular discs [27].

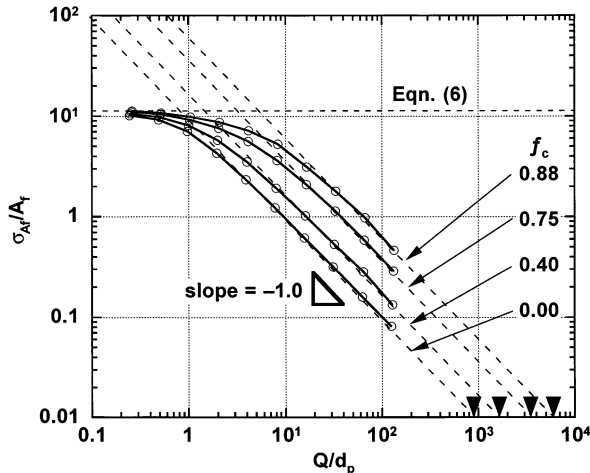


Fig. 8. MSAAF plot for simulated microstructures, showing the variation in σ_{A_f}/A_f with increasing Q/d_p for different values of clustering factor between $f_c = 0$ (i.e. random, non-overlapping) and $f_c = 0.88$ (highly clustered). Small arrows on the lower right horizontal axis indicate values of $L_H(0.01)$. ($A_f = 0.8\%$, $N = 10\,000$).

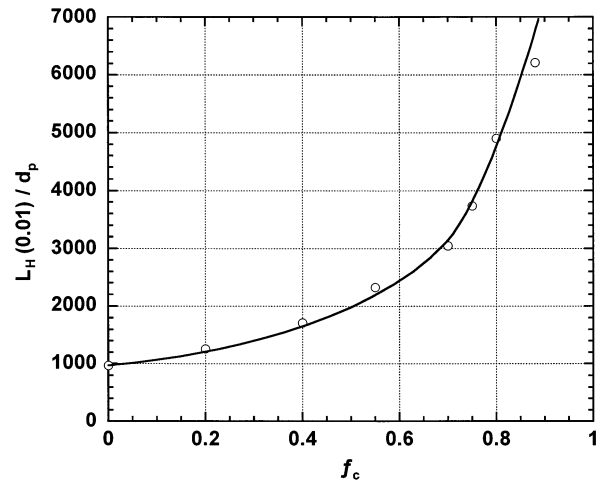


Fig. 9. Variation of $L_H(0.01)/d_p$ with increasing clustering factor, f_c . The line is a non-parametric curve fit through the data. ($A_f = 0.8\%$, $N = 10\,000$).

2.4. Multi-scale analysis of area fraction in clustered microstructures with monosized particles

Often, experimentally obtained discontinuously reinforced composite microstructures contain localized regions, where the variation in area fraction of particles is much higher than would be expected based on random, non-overlapping particle placement [2]. These ‘clustered’ microstructures can also be simulated by the computer code described in Section 2.1. The clusters are formed, when a pre-determined proportion of the particles are placed as close as possible to existing particle positions, instead of at random coordinates, again without any particles overlapping. The ratio of the number of particles that are placed in clusters to the number that are placed at random coordinates within the remaining area is defined as the clustering factor, f_c .

Fig. 8 shows the relationship between σ_{A_f}/A_f and Q/d_p for simulated clustered microstructures having values of clustering factor between $f_c = 0$ (i.e. random, non-overlapping) and $f_c = 0.88$ (highly clustered). Each of the microstructures contains 10 000 particles, at an overall area fraction of $A_f = 0.8\%$. Even for the highly clustered microstructures (i.e. $f_c \rightarrow 1.0$) there is still a quilt size above which the slope becomes -1 , as predicted by Poisson statistics for the case of random, non-overlapping particles. The quilt size at which this occurs increases with increasing f_c at a constant area fraction of reinforcement.

Extrapolation of the curves to the horizontal axis at $\sigma_{A_f}/A_f = 0.01$ yields a value for $L_H(0.01)/d_p$, which increases systematically with f_c , as shown in Fig. 9.

2.4.1. Effect of area fraction on spatial heterogeneity

Consider the difference between highly clustered microstructures with low and high area fractions of rein-

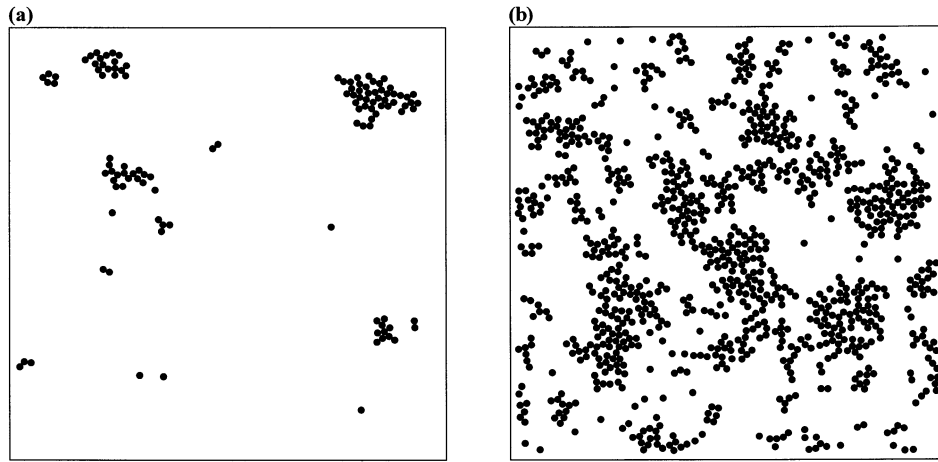


Fig. 10. Clustered microstructures (a) $f_c = 0.8$, $A_r = 0.8\%$, and (b) $f_c = 0.8$, $A_r = 20\%$. Both microstructures are shown at the same magnification.

forcements. The former will have the potential for increased levels of spatial heterogeneity due to the greater available space in which clusters can form. This may in turn increase L_H . For example, Fig. 10 shows two microstructures that have similar levels of clustering, f_c but different area fractions ($A_r = 0.8\%$ vs. $A_r = 20\%$). The microstructure with $A_r = 20\%$ was chosen in order to represent the level of reinforcement volume fraction typically observed in actual discontinuously reinforced MMC materials, although in practice, the particle spatial distributions are usually more homogeneous than in this example.

Fig. 11 shows the effect on $L_H(0.01)/d_p$ of increasing the clustering factor for monosize particles with increasing area fractions from the dilute (Poisson) case ($A_r = 0.8\%$) up to $A_r = 20\%$. From the figure, we can see that there is a large increase in $L_H(0.01)/d_p$ as we reduce the area fraction from 20% to 0.8%, especially at the higher levels of clustering. Conversely, at equivalent levels of clustering, a microstructure containing a higher area fraction of particles will be more uniform than one containing fewer particles. This is simply an effect of there being less room in which to arrange the particles as the area fraction is increased, i.e., there are fewer possible ways of packing in the particles as we approach the higher area fractions, therefore, large local variations in area fraction become increasingly unlikely (Section 2.3.1) irrespective of the imposed clustering factor.

3. Effect of particle size distribution on spatial heterogeneity

In the preceding sections, we have relied on the assumption of having monosized particles. However, experimental discontinuously reinforced MMC mi-

crostructures will usually contain particles with a distribution of sizes about some mean size. Experimental particle size distributions are often characterized in terms of log-normal statistics rather than normal (i.e. Gaussian) statistics.

3.1. Log-normal statistics for characterizing particle size distributions

The log-normal probability distribution function [28] is given in Eq. (9).

$$p(d_p) = \frac{1}{a} \exp[-(\ln d_p - \ln d_g)^2/b], \quad (9)$$

where

$$a = \sqrt{2\pi} \ln \sigma_g, \quad (10)$$

and

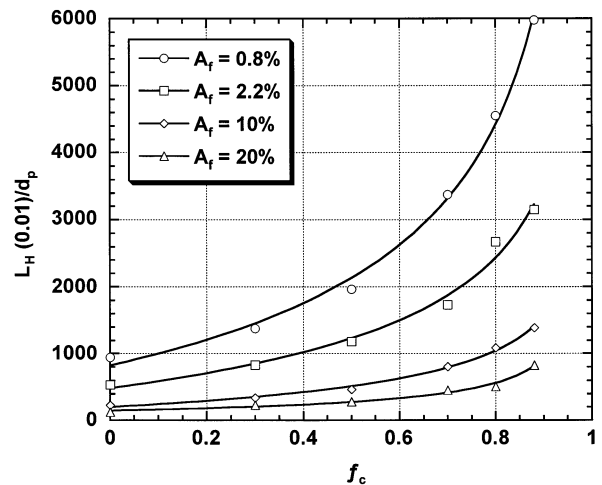


Fig. 11. Effect of increasing clustering factor, f_c , on homogeneous length scale, $L_H(0.01)$, for different area fractions of monosize particles. ($N = 10\,000$, $A_r = 0.8\%$, 2.2% , 10% , 20%).

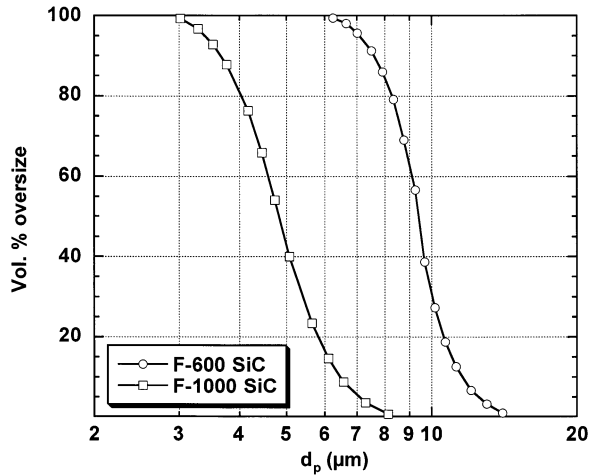


Fig. 12. Cumulative probability plots for two experimental particle size distributions; (Norton F-600 and F-1000 SiC powders) [30].

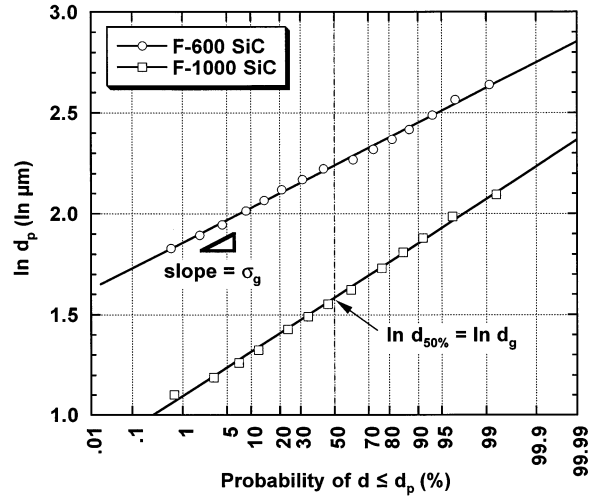


Fig. 13. Log-probability plots for two experimental particle size distributions (Norton F-600 and F-1000 SiC powders). Note straight-line fit through data, indicating lognormal statistics.

Table 1
Parameters from curve-fitting the F-600 and F-1000 SiC particle size data, using log-normal statistics^a

Parameter	F-600 SiC	F-1000 SiC
d_g (μm)	9.4	4.9
$\ln \sigma_g$ ($\ln \mu\text{m}$)	0.165	0.210
R	0.9987	0.9988

^a R is the linear correlation coefficient.

$$b = 2 \ln^2 \sigma_g. \quad (11)$$

In these equations, $p(d_p)$ is the probability of finding a particle of diameter d_p , d_g is the geometric mean of the distribution of d_p and σ_g is the geometric mean deviation, as defined by the following equations:

$$\ln d_g = \frac{1}{n} \ln \left(\prod_{i=1}^n d_i \right) = \frac{1}{n} \left[\sum_{i=1}^n \ln d_i \right], \quad (12)$$

$$\ln^2 \sigma_g = \frac{1}{n-1} \left[\sum_{i=1}^n (\ln d_i - \ln d_g)^2 \right]. \quad (13)$$

These parameters can be put into context using commercially available data for particle size distributions. Fig. 12 shows cumulative probability plots⁴ representative of two commercially available SiC powders commonly used in the fabrication of discontinuously reinforced MMC materials (Norton F-600 and F-1000) [30]. The two parameters d_g and σ_g (which uniquely describe a log-normal distribution) are obtained by plotting the cumulative probability data in the form of a log-probability plot, as shown in Fig. 13. (The straight line fit through the data is sufficient to indicate adherence to log-normal statistics [22].)

Table 1 contains the two statistical parameters obtained from Fig. 13, for both particle size distributions, F-600 and F-1000. We can see that the larger mean diameter F-600 powder has a narrower distribution of particle sizes relative to the mean particle size, d_g , as indicated by the smaller value of σ_g vs. that of the F-1000 powder. The effect on the MSAF plot of a variation in particle size will now be addressed, using these two distributions of particle size as specific examples.

3.2. Simulating particle populations

Due to stereological effects [31], there will be a noticeable difference between the actual distribution of powder particle diameters and the distribution of measured particle diameters that results from a random 2-D section through the discontinuously reinforced composite material. The parameters d_g and σ_g that fully describe the particle size distributions for the F-600 and F-1000 SiC powders must therefore be modified in order to produce an accurate 2-D representation of the simulated 3-D composite microstructure. If we assume a log-normal distribution of particle diameters in the 2-D section, we can use the result of Fullman [32] to obtain the appropriate statistical parameters (d_g and σ_g) for the 2-D distribution, based on the following observation:

$$\bar{d} = \frac{\pi}{2\bar{m}}. \quad (14)$$

Here, \bar{d} is the true average particle diameter, and \bar{m} is the average of the reciprocals of the particle diameters in the corresponding 2-D section. Each particle diameter must be reduced by a constant factor ($\alpha < 1$) in order for Eq. (14) to be true. This factor (which is found to be a function of d_g and σ_g), must be calculated

⁴ Obtained using the Coulter counting method [29].

in each different case. Once α has been identified, d_g^{2D} and σ_g^{2D} can then be calculated for the 2-D distribution. For lognormal distributions, the following simple relationships will always apply:

$$\sigma_g^{2D} = \sigma_g, \tag{15}$$

$$\ln d_g^{2D} = \ln \alpha + \ln d_g. \tag{16}$$

Fig. 14(a) and (b) show histograms of 2-D particle size data for two simulated 10 000 particle populations, obtained in this manner, using the log-normal statistics of the F-600 and F-1000 SiC powders (Table 1). Notice that neither of the distributions are symmetrical about d_g , but have a slight tail to the right, in accordance with a log-normal distribution.

Fig. 15(a) and (b) shows the two simulated microstructures at the same magnification. The larger

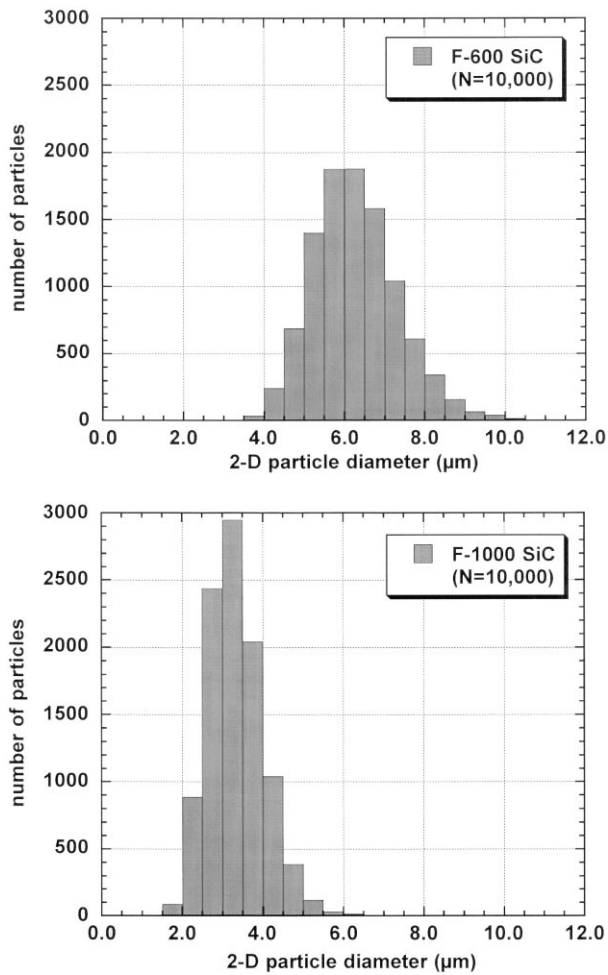


Fig. 14. (a) Histogram showing apparent 2-D particle size distribution expected for a random planar section through a simulated 10 000 particle population, according to log-normal statistics of F-600 SiC powder ($d_g = 9.4 \mu\text{m}$, $d_g^{2D} = 6.2 \mu\text{m}$, $\alpha = 0.655$, $\ln \sigma_g = 0.165$). (b) Histogram showing apparent 2-D particle size distribution expected for a random planar section through a simulated 10 000 particle population, according to log-normal statistics of F-1000 SiC powder ($d_g = 4.9 \mu\text{m}$, $d_g^{2D} = 3.3 \mu\text{m}$, $\alpha = 0.665$, $\ln \sigma_g = 0.210$).

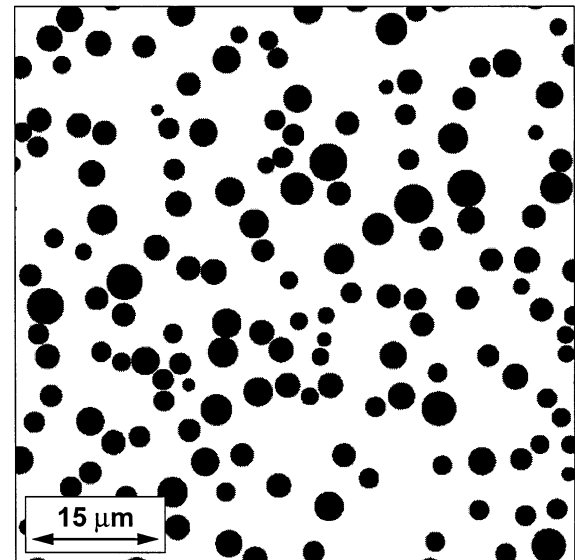
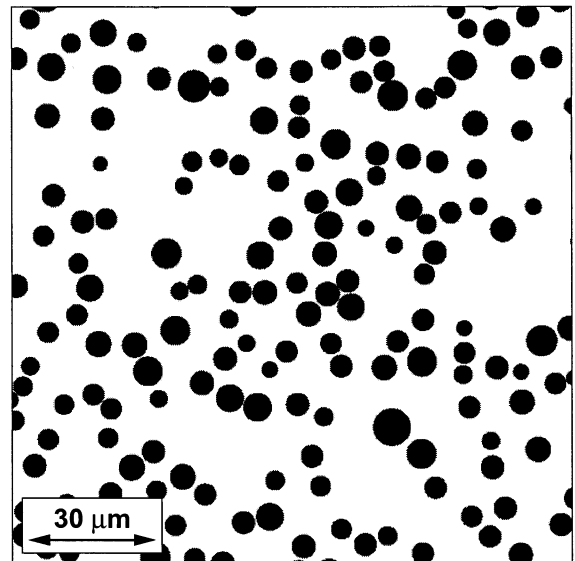


Fig. 15. (a) Portion of simulated microstructure that contained 10 000 (F-600) SiC powder particles ($d_g = 9.4 \mu\text{m}$, $d_g^{2D} = 6.2 \mu\text{m}$, $\alpha = 0.655$, $\ln \sigma_g = 0.165$). Random, non-overlapping particle placement, $f_c = 0$. (b) Portion of simulated microstructure that contained 10 000 (F-1000) SiC powder particles ($d_g = 4.9 \mu\text{m}$, $d_g^{2D} = 3.3 \mu\text{m}$, $\alpha = 0.665$, $\ln \sigma_g = 0.210$). Random, non-overlapping particle placement, $f_c = 0$.

variability in particle sizes of the F-1000 powder vs. the F-600 powder is quite apparent. Fig. 16 shows two MSAAF plots obtained from the F-600 and F-1000 simulated microstructures, using random, non-interacting particle placement. Each microstructure contained 10 000 particles at an area fraction of $A_f = 20\%$, which was chosen to represent a typical MMC volume fraction. The figure shows that there is negligible difference between the two MSAAF curves. Each curve has a slope of -1.0 over the linear portion, and have similar

values for $L_H(0.01)/d_p$ ($\approx 1 \times 10^2$). The effect of different particle size distributions is therefore expected to be insignificant at the levels of σ_g expected in practice.

4. Multi-scale analysis of area fraction in experimental discontinuously reinforced metallic matrix composite microstructures

The preceding sections have dealt exclusively with simulated microstructures. In this section, the MSAAF analysis is extended to real microstructures, obtained from metallographic sectioning of experimental discontinuously reinforced aluminum (DRA) materials. The two materials chosen for comparison were produced under identical (P/M) processing conditions [33] and comprised a 2080-Al matrix with 20 vol% of either F-600 or F-1000 SiC particles as reinforcement. In order to obtain high-resolution digital optical micrographs of the two DRA materials after sectioning and polishing, a montage technique [34] was employed, whereby multiple adjacent sub-images were captured digitally and reconstructed into one final image, using a commercial desktop package.⁵ This effectively de-coupled the available resolution and the field-of-view, which enabled pixel re-sampling down to small values of Q/d_p .

4.1. Image processing

A sequence of image processing filters [35] was employed in order to obtain consistent binary (black and

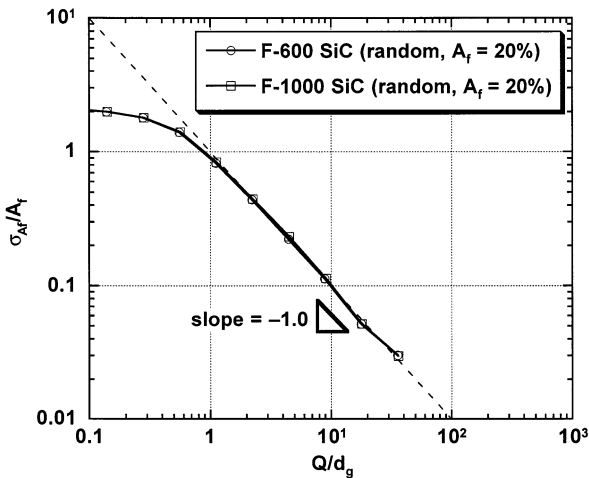


Fig. 16. MSAAF plot for two random, non-overlapping distributions of particles, simulating discontinuously reinforced MMC materials made with the F-600 and F-1000 SiC powders. ($N = 10\,000$, $A_f = 20\%$). Note that the quilt size, Q is normalized with respect to the geometric mean diameter, d_g , and that the two curves overlap.

⁵ Adobe Photoshop 5.5.

white) images from the digital optical micrographs of experimental DRA microstructures. Fig. 17(a)–(e) show the sequence of operations carried out on a portion of such an image. The resulting binary image (i.e. Fig. 17(e)) is then used as an input image for the MSAAF re-sampling procedure (Section 2.2).

4.2. Multi-scale analysis of area fraction of experimental discontinuously reinforced aluminum microstructures

Fig. 18 compares the MSAAF plot obtained from the as image-processed experimental DRA microstructure shown in Fig. 17(e) ($A_f = 20\%$, F-600 SiC reinforcement) with that of a simulation using random, non-interacting particle placement, ($f_c = 0$, $A_f = 20\%$, F-600 SiC particle size distribution). Note that in both cases the quilt size, Q , is normalized with respect to the geometric mean of the particle size distribution, d_g .

The figure shows that although both MSAAF plots show a slope of -1 in the linear region, the experimental DRA microstructure has a higher $L_H(0.01)/d_p$ than the simulation, i.e., it is more heterogeneous. Using a value of $d_g = 9.4\ \mu\text{m}$ for the F-600 SiC powder, we can extrapolate to a value of $L_H(0.01) \approx 1.2\ \text{mm}$ in the DRA material, versus a value of $L_H(0.01) \approx 0.74\ \text{mm}$ in the random simulation.

Fig. 19(a) and (b) are digital optical micrographs that compare regions of the experimental F-600 and F-1000 DRA microstructures. Although the two micrographs are shown at different magnifications, the fields of view are equivalent, due to the different mean particle sizes in each material. Qualitatively, there is increased heterogeneity in the distribution of the reinforcement in the F-1000 DRA, when compared to the F-600 material, and evidence of extensive clustering of the particles. In order to quantify the level of heterogeneity in this microstructure, an MSAAF plot obtained from the experimental F-1000 DRA material is compared with that of a simulation using random, non-interacting particle placement, ($f_c = 0$, $A_f = 20\%$, F-1000 SiC particle size distribution), Fig. 20.

The slope of the MSAAF plot for the F-1000 DRA material in the measured range is much shallower than that of the F-600 DRA, i.e. -0.67 versus -1.0 . This implies a greater level of heterogeneity, since the F-1000 material shows a greater variability in local area fraction than the F-600 material over the measured length scales. The homogeneous length scale is also increased, i.e., $d_g = 4.9\ \mu\text{m}$ for the F-1000 SiC powder, therefore $L_H(0.01) \approx 3.6\ \text{mm}$ in the F-600 DRA compared with $L_H(0.01) \approx 1.2\ \text{mm}$ in the F-600 DRA. It should be noted, however, that we are extrapolating significantly from the measured data in the F-600 case. Even though the initially lower slope suggests stronger heterogeneity than the F-600 material at length scales below $\sim 50\ d_g$,

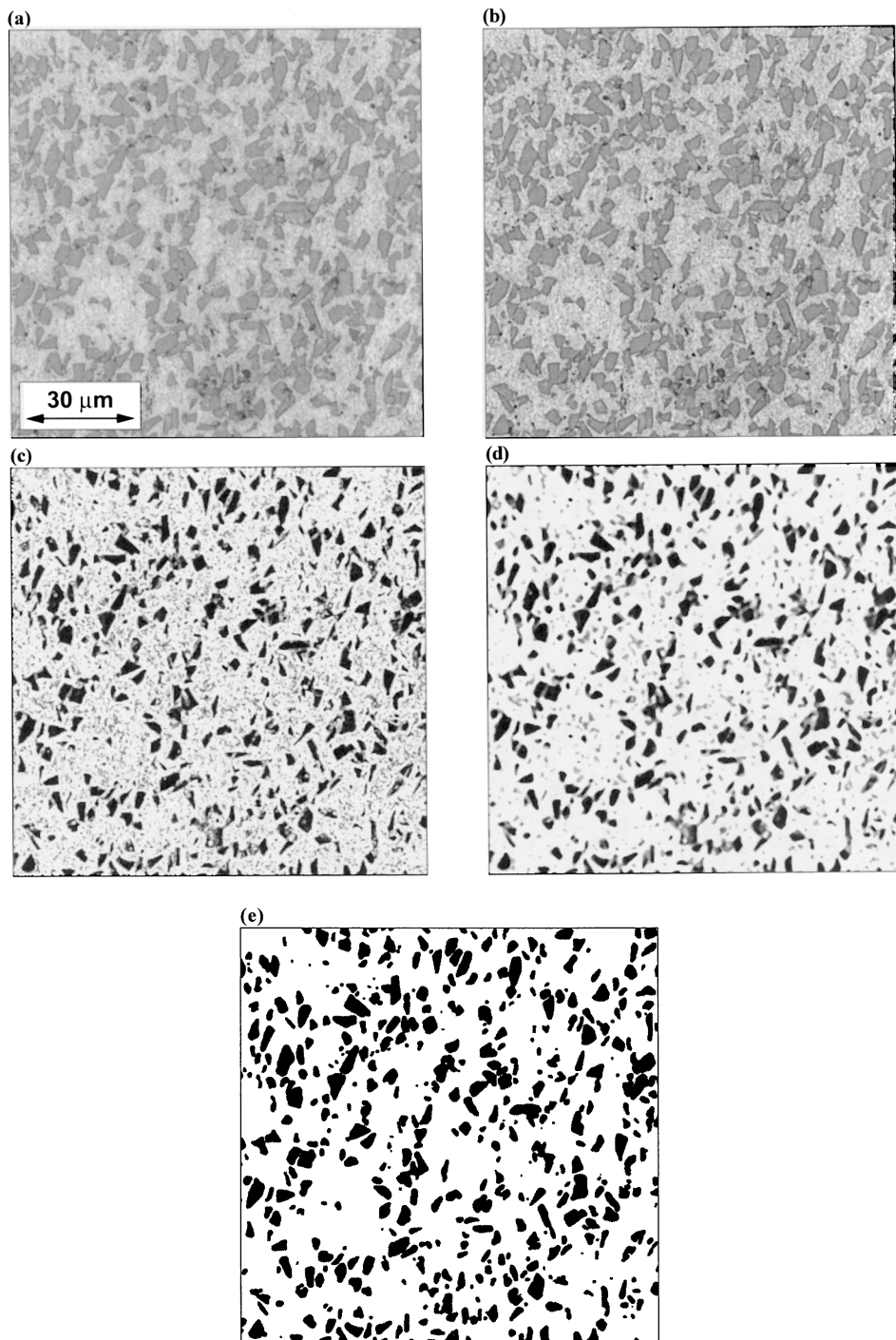


Fig. 17. (a)–(e): Sequential image processing operations [35] carried out on a 512×512 pixel digital optical micrograph of a 20 vol% F-600 SiC reinforced aluminum MMC; (a) original micrograph, (b) 'unsharp mask' applied, (c) 'Haralick 2' filter applied, (d) median filter (2 pixel radius) applied, and (e) final thresholded (binary) image.

it is possible that the curve may eventually assume a slope of -1.0 at larger quilt sizes. This phenomenon was clearly demonstrated in the simulated random, non-overlapping microstructures with increasing degrees of clustering (Fig. 8), where the slope of the MSAAF curves became -1.0 at length scales much larger than the scale of the clusters.

4.3. Modeling of experimental discontinuously reinforced aluminum microstructures

Since the slope of the MSAAF plot for the experimental F-600 DRA material is -1.0 , it is possible to model this microstructure using the clustering factor, f_c , as a single fitting parameter. Whilst maintaining the

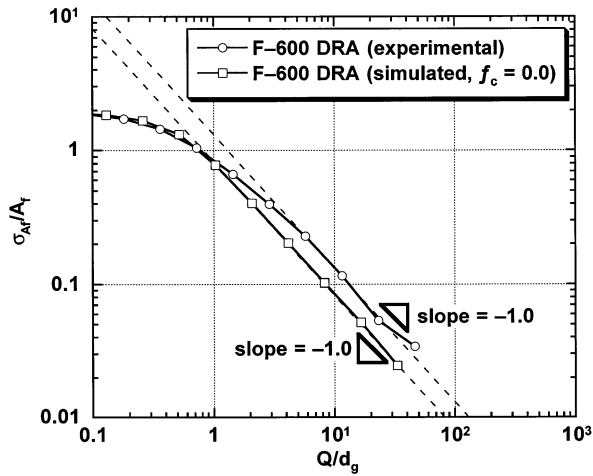


Fig. 18. MSAAF plot comparing an experimental F-600 DRA microstructure and a simulated microstructure using F-600 SiC particle size distribution ($d_g = 9.4 \mu\text{m}$) and a random, non-overlapping particle placement routine ($f_c = 0$). In each case, $A_f = 20\%$.

same A_f and particle size distribution, the clustering factor is increased from a random, non-interacting case ($f_c = 0$) until the modeled curve lies on top of the experimental curve. For the F-600 DRA material, this occurs with a clustering factor of $f_c = 0.3$, suggesting that the F-600 DRA material is *slightly* clustered, as shown in Fig. 21.

Fig. 22(a) and (b) compare images of the experimental F-600 DRA microstructure with the simulated microstructure ($f_c = 0.3$), at the same magnification. The only significant difference appears at the smaller length scales, i.e. below the mean particle size, d_g . In the experimental DRA microstructure, a greater number of smaller particles have been sectioned. This may account for the slight difference between the

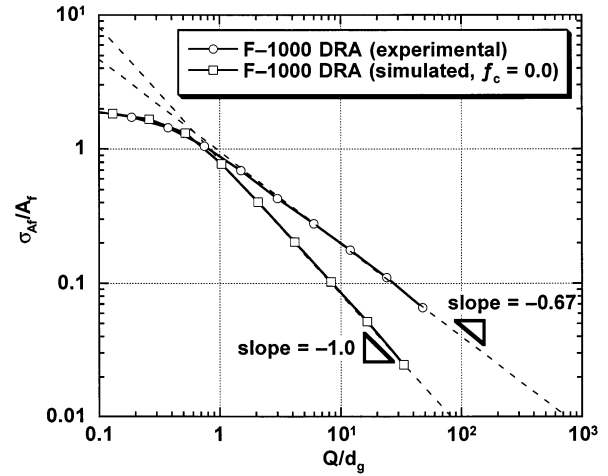


Fig. 20. MSAAF plot comparing the experimental F-1000 DRA microstructure and a simulated microstructure using F-1000 SiC particle size distribution ($d_g = 4.9 \mu\text{m}$) with a random, non-overlapping particle placement routine ($f_c = 0$). In each case, $A_f = 20\%$.

shapes of the MSAAF plots, at quilt sizes smaller than Q/d_g .

The simulated microstructures produced using the techniques described in Section 2.1 and Section 2.4 all have MSAAF plots with slopes of -1.0 . It is postulated that the shallower slope (-0.67) measured for the F-1000 DRA material may be indicative of multi-scalar (i.e. fractal [36]) microstructural phenomena, e.g. the formation of ‘super-clusters’, containing clusters of clusters. This behavior is not captured in the simple modeling scheme, and so no attempt will be made to model the F-1000 microstructure. Future work, focusing on producing model microstructures using a cellular automaton multi-scalar approach may be fruitful in this respect.

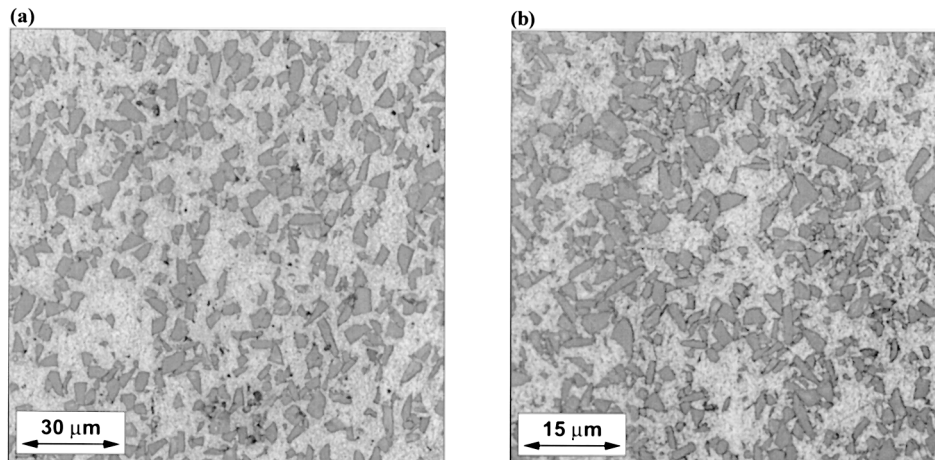


Fig. 19. Digital optical micrographs comparing (a) F-600 and (b) F-1000 DRA microstructures. Notice increased spatial heterogeneity of reinforcement distribution in F-1000 DRA, (relative to F-600 material), and evidence of extensive particle clustering.

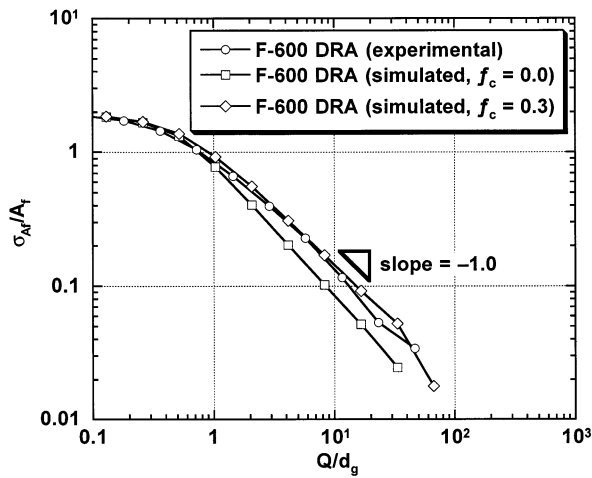


Fig. 21. MSAAF plot comparing the experimental F-600 DRA material and simulated microstructures using the F-600 SiC particle size distribution ($d_g = 9.4 \mu\text{m}$) with clustering factors $f_c = 0$ and $f_c = 0.3$. In each case, $A_f = 20\%$.

5. Relevance of multi-scale analysis of area fraction for predicting mechanical properties of discontinuously reinforced metallic matrix composite materials

5.1. Design allowables

Material property values that are specified for component design purposes are typically chosen to be minimum expected values, obtained via strict statistical analyses of property data from tests carried out on a large number of identical specimens. Property values obtained in this way are called design allowables [37]. In this respect, the amount of inherent variability in material data can sometimes be more important in specifying the allowable than the mean value of the property, as illustrated in Fig. 23 for a hypothetical material property.

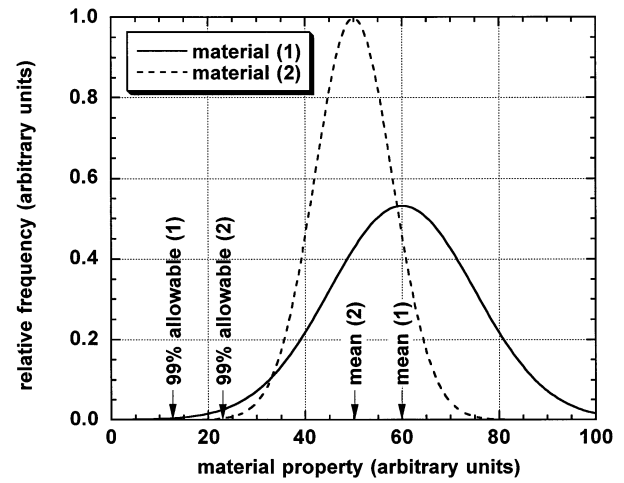


Fig. 23. Plot showing reduction in design allowable due to increased variability in a hypothetical mechanical property. Material (1) has a higher mean property than material (2) but the 99% design allowable for material (1) is lower, due to larger spread in the data.

Mechanical properties in discontinuously reinforced MMCs typically show a fair amount of variation [38,39]. However, it seems reasonable to conjecture that in these materials, properties such as tensile strength and ductility (and possibly also fatigue and fracture toughness) should be correlated in a deterministic way with the volume fraction, distribution, size and morphology of reinforcement. The variability observed for composite material properties with identical volume fractions might therefore be attributed to variability in microstructure, particularly in the spatial distribution of the reinforcing particles. By using the MSAAF technique, we have carefully shown that the amount of variability in local particle volume fraction (as characterized by σ_{A_f}/A_f) is not only a function of the degree of clustering but it also varies with length scale (quilt size), as demonstrated by the significant horizontal shift in

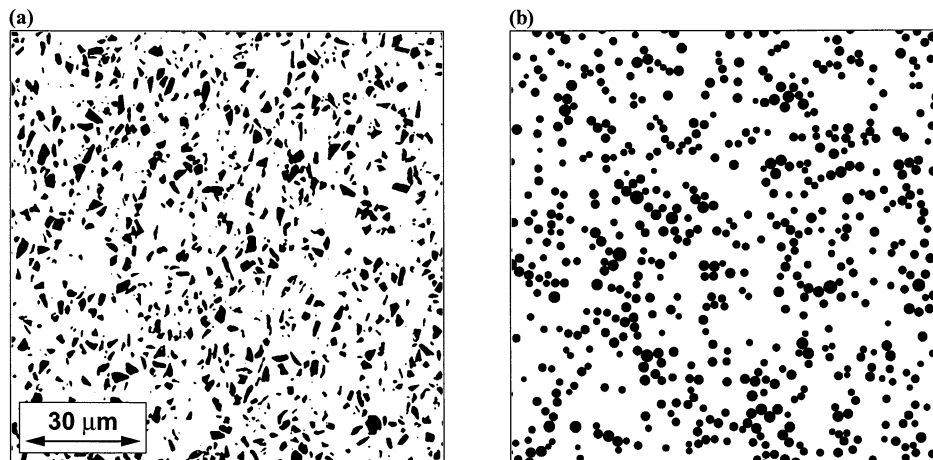


Fig. 22. Comparing (a) experimental and (b) simulated DRA microstructures at the same magnification. Simulated microstructure has clustering factor, $f_c = 0.3$ ($A_f = 20\%$).

the MSAAF curves shown in Fig. 8. It is therefore important to consider over what length scale (or scales) each different failure mechanism is likely to be operating.

Plane-strain fracture toughness (K_{IC}) is one such material property that shows a much larger amount of scatter in discontinuously reinforced MMCs than is typically seen in the monolithic metals. For example, variability in K_{IC} data for DRA materials containing 20 vol% SiC can be as high as 30% [40], whereas variability in K_{IC} data for a high-strength Al alloy (compact tension specimen geometry) has been reported as low as 3% [41,42]. An obvious candidate length scale for the fracture mechanism might be the size of the plastic zone (R_p) ahead of the advancing crack tip. An upper limit [43] for R_p is given by:

$$R_p \approx 0.155 \left(\frac{K_{IC}}{\sigma_Y} \right)^2. \quad (17)$$

Using a value [33] of $\sigma_Y = 522$ MPa and a typical value [44] of $K_{IC} = 15 \text{ MPa}\sqrt{m}$, we obtain an estimate of $R_p \approx 130 \mu\text{m}$ for the F-600 DRA material. Referring to Fig. 18, the point-to-point variation in area fraction (i.e. σ_{A_f}/A_f) at this length scale would be around 9% in this material. Similarly, using $K_{IC} = 15 \text{ MPa}\sqrt{m}$ for the F-1000 DRA material ($\sigma_Y = 539$ MPa [33], $R_p \approx 120 \mu\text{m}$), the point-to-point variation in area fraction is around 11% (Fig. 20). It is proposed that this measured variability in area fraction may contribute (at least in part) into the measured variability in K_{IC} , assuming that a deterministic relationship does exist between fracture toughness and reinforcement volume fraction. This therefore provides a tentative link between a microscale phenomenon (i.e. variation in area fraction at the length scale of the plastic zone size) and the macroscopic property, K_{IC} . Additionally, the slight trend of a higher variability in area fraction for the F-1000 material may translate into a more conservative value for the design allowable than for the F-600 material, even though the F-1000 material may possess a higher mean toughness.⁶

Unfortunately, due to overwhelming scatter [45] in the experimental data for measured K_{IC} values, no clear empirical relationship has been established between fracture toughness and reinforcement volume fraction. Fracture toughness can not therefore be predicted a priori for a DRA material that has a known variability in area fraction. However, through improved powder blending techniques or other methods [46] it should be possible to improve the spatial distribution of reinforcement particles throughout the microstructure, (i.e. eliminate particle clustering and so reduce L_H), and gain an

improvement in K_{IC} . It is proposed that only by the reduction of microstructural heterogeneity at the relevant length scale can we hope to improve the fracture properties of these materials. Future work will concentrate on correlating K_{IC} data measured in DRA materials containing different particle spatial distributions, with relevant microstructural parameters obtained from the MSAAF technique.

5.2. Matrix coating of particles

In an effort to produce discontinuously reinforced MMCs with enhanced levels of homogeneity, an experimental program has recently been initiated whereby ceramic reinforcement particles will be coated with a continuous layer of matrix alloy prior to incorporation into fully dense composite materials [46]. The purpose of the coating is to increase the separation between neighboring particles, and so preclude particle–particle contact. Matrix coating of particles (MCP) can be carried out by a number of processes, including fast fluidized-bed chemical vapor deposition [47], electrochemical plating and non-aqueous polyol salt deposition techniques [48]. A strong potential exists for increasing the homogeneity of particle spatial distributions in discontinuously reinforced MMCs by the use of these techniques, along with an expected enhancement in fracture properties. Furthermore, the process of uniformly coating ceramic particles with matrix material is attractive not only in traditional P/M billet materials, but also in direct powder forging [49] and pressure-infiltration cast [50] products.

It is possible to model the effect on the overall microstructural homogeneity of adding a layer of matrix material to each particle, by using the computer code to simulate MCP–DRA microstructures. The code is modified to assign a fixed exclusion distance (equal to twice the coating thickness) around each particle as it is placed in the microstructure. Particles are placed using the same rules as before, except in the MCP–DRA simulation, no particles will be placed with less than the minimum edge-to-edge separation allowed by the exclusion distance.⁷

Fig. 24(a) and (b) shows the results of such treatments applied to the F-600 and F-1000 simulated microstructures obtained before (Fig. 15(a) and (b)). The particles were modeled as having a matrix coating thickness of $1.0 \mu\text{m}$, and an overall area fraction of 20%. From the simulation, we can see a greater effect on the homogeneity of the distribution for the smaller (F-1000) SiC than the F-600 SiC powder, simply due to the fixed thickness of the coating layer. Thus the MCP

⁶ Although K_{IC} data are not available, the tensile yield and ultimate strengths were measured [33] to be slightly higher in the F-1000 material than in the F-600 material.

⁷ The 2-D jamming limit of $A_f = 0.547$ will still be in effect, but here it refers to an effective area fraction comprising the total particle area fraction plus the area fraction from the matrix coating itself.

technique is predicted to make the greatest improvements on DRA materials containing smaller reinforcing particles, for a given matrix coating thickness. Indeed, the technique may be invaluable in the effort to produce discontinuously reinforced MMCs with very small ($\leq 1 \mu\text{m}$ diameter) reinforcements (B.S. Majumdar, personal communication) without introducing particle clusters.

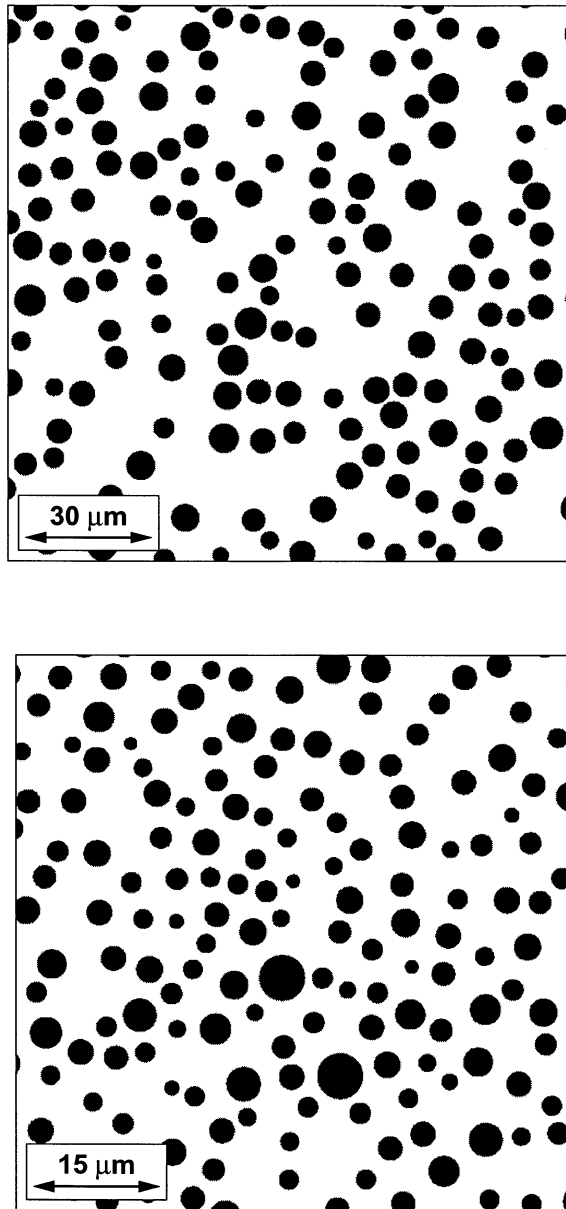


Fig. 24. (a) Portion of a simulated MCP–DRA microstructure ($A_f = 20\%$) that contained 10 000 F-600 SiC powder particles ($d_g = 9.4 \mu\text{m}$) with a matrix coating layer thickness of $1.0 \mu\text{m}$. (Random, non-overlapping particle placement, $f_c = 0$.) (b) Portion of a simulated MCP–DRA microstructure ($A_f = 20\%$) that contained 10 000 F-1000 SiC powder particles ($d_g = 4.9 \mu\text{m}$) with a matrix coating layer thickness of $1.0 \mu\text{m}$. (Random, non-overlapping particle placement, $f_c = 0$.)

6. Conclusions

We have demonstrated that by using the MSAAF technique, it is possible to assign a new microstructural parameter, the homogeneous length scale, L_H , to distributed heterogeneous systems. This parameter describes the statistical variation in the area fraction of the distributed second phase. The length scales that can be interrogated with the MSAAF technique range from below the particle diameter up to the size of the specimen, although the information obtained at length scales below the particle diameter is somewhat limited. Statistical information of this sort is obtained without resorting to tessellation techniques or relying on manual separation of the particles, therefore an improvement in performance over these techniques is anticipated. The results from MSAAF carried out on low- A_f particle ensembles agree favorably with analytical expressions for Poisson distributions of points in a plane, validating the technique. The technique also correctly predicts the 2-D “jamming limit” approached with high- A_f random, non-overlapping synthetic microstructures.

When the MSAAF technique is used to characterize two different experimental DRA materials (Al 2080/SiC/20_p containing either F-600 or F-1000 SiC particles), it correctly identifies the relative amounts of spatial heterogeneity observed in the different microstructures. This suggests that the technique may be useful for quality assurance and process control of DRA microstructures in the future.

The ability to characterize the amount of spatial variability in distributed multi-phase systems, such as particulate-reinforced MMCs, is the first step towards establishing a correlation between microstructure and mechanical properties in these systems. Experiments are planned in which the MSAAF analysis will be correlated with the results of DRA fracture toughness tests, using samples with different degrees of spatial heterogeneity. It is hoped that these experiments will yield correlations between the statistical distribution of local volume fractions and measured fracture toughness data.

Acknowledgements

The authors wish to acknowledge the following individuals for their valuable contributions in many different aspects of this work: Alan Frazier, Dr Joel Philliber, Dr Nikhilesh Chawla, and Dr Rick Everett. This work was supported by the Air Force Research Laboratory under Contract no. F33615-96-C-5258.

References

- [1] S.F. Corbin, D.S. Wilkinson, *Acta Metall. Mater.* 42 (1994) 1311.
- [2] A.M. Murphy, S.J. Howard, T.W. Clyne, *Mat. Sci. Tech.* 14 (1998) 959.
- [3] A.R. Vaida, J.J. Lewandowski, *Mater. Sci. Eng.* A220 (1996) 85.
- [4] S. Tao, J.D. Boyd, Proceedings of the ASM 1993 Materials Congress, Pittsburgh, PA, October 17–21, 1993 ASM International, Materials Park, OH, 1993, p. 29.
- [5] J.J. Lewandowski, C. Liu, *Mater. Sci. Eng.* A107 (1989) 241.
- [6] H. Schwarz, H.E. Exner, *J. Microsc.* 129 (1983) 155.
- [7] T.M. Osman, J.J. Lewandowski, W.H. Hunt Jr., Fabrication of Particulates Reinforced Metal Composites: Proceedings of an International Conference, Montréal, Québec, Canada, 17–24 September, 1990, ASM International, Materials Park, OH, 1990, p. 209.
- [8] W.H. Hunt Jr., O. Richmond, R.D. Young, Proceedings of ICCM-6/ECCM-2, London, UK, 1987, Elsevier Applied Science, 1987, p. 2.209.
- [9] J. Boselli, P.D. Pitcher, P.J. Gregson, I. Sinclair, *J. Microscopy* 195 (1999) 104.
- [10] W.A. Spitzig, J.F. Kelly, O. Richmond, *Metallography* 18 (1985) 235.
- [11] M. Li, S. Ghosh, O. Richmond, H. Weiland, T.N. Rouns, *Mater. Sci. Eng.* A256 (1999) 153.
- [12] M. Li, S. Ghosh, O. Richmond, H. Weiland, T.N. Rouns, *Mater. Sci. Eng.* A266 (1999) 221.
- [13] B. Lu, S. Torquato, *J. Chem. Phys.* 93 (1990) 3452.
- [14] J. Quintanilla, S. Torquato, *J. Chem. Phys.* 106 (1997) 2741.
- [15] J.G. Berryman, *J. Appl. Phys.* 57 (1985) 2374.
- [16] J.K. Shang, W. Yu, R.O. Ritchie, *Mater. Sci. Eng.* A102 (1988) 181.
- [17] T. Lin, A.G. Evans, R.O. Ritchie, *Acta Metall.* 34 (1986) 2205.
- [18] J.E. Hilliard, J.W. Cahn, *Trans. Met. Soc. AIME* 221 (1961) 344.
- [19] D. van Hille, S. Bengtsson, R. Warren, *Compos. Sci. Tech.* 35 (1989) 195.
- [20] C. Lantuéjoul, *Acta Stereologica* 6 (1987) 103.
- [21] J.P. Rigaut, C. Lantuéjoul, F. Deverly, *Acta Stereologica* 6 (1987) 107.
- [22] W. Mendenhall, T. Sincich, *Statistics for Engineering and the Sciences*, Prentice Hall, Englewood Cliffs, NJ, 1995.
- [23] R.K. Everett, DISTRIB-code 6382 v.1.0 (True BASIC code), Naval Research Laboratory, Washington, DC, 1992.
- [24] M. Robbeloth, DISTRIB2 v.1.0 (Pascal code), AFRL/MLLM, Wright-Patterson AFB, 1999.
- [25] A. Frazier, DM4 v.4.0 (C++ code), AFRL, Wright-Patterson AFB, 2000.
- [26] C.A. Smith, DWA Aluminum Composites, personal communication, 2000.
- [27] E.L. Hinrichsen, J. Feder, T. Jøssang, *J. Stat. Phys.* 44 (1986) 793.
- [28] C.H. Murphy, *Handbook of Particle Sampling and Analysis Methods*, VCI, 1984.
- [29] FEPA Standard for Bonded Abrasive Grains of Fused Aluminium Oxide and Silicon Carbide, (FEPA 42-GB-1984 R1993), Federation of the European Producers of Abrasives, 1993.
- [30] Crystolon® Norton Silicon Carbide Technical Bulletin, Saint-Gobain Industrial Ceramics, Worcester, MA, 1999.
- [31] E.E. Underwood, *Quantitative Stereology*, Addison-Wesley, Reading, MA, 1970.
- [32] R.L. Fullman, *Trans. AIME* 197 (1953) 447.
- [33] N. Chawla, C. Andres, J.W. Jones, J.E. Allison, *Met. Mat. Trans.* 29A (1998) 2843.
- [34] J.A. Philliber, Sandia Livermore Laboratory, personal communication, 1999.
- [35] J.C. Russ, *The Image Processing Tool Kit v.2.10 (CD ROM) Reindeer Games*, 1996–1997.
- [36] B.B. Mandelbrot, *The Fractal Geometry of Nature*, W.H. Freeman, San Francisco, CA, 1982.
- [37] *Metallic Materials and Elements for Aerospace Vehicle Structures: MIL-HDBK-5H*, AFRL/MLSC, Wright-Patterson AFB, OH, 1998.
- [38] W.A. Logsdon, P.K. Liaw, *Engng. Fracture Mech.* 24 (1986) 737.
- [39] W.H. Hunt Jr., T.M. Osman, J.J. Lewandowski, *JOM* 45 (1993) 30.
- [40] J.J. Lewandowski, Fatigue and fracture of particulate MMCs, in: A. Kelly, C. Zweben (Eds.), *Comprehensive Composite Materials*, vol. 3, Elsevier, Amsterdam, 2000, p. 151.
- [41] D.E. McCabe, *JOM* 7 (1972) 449.
- [42] Standard Test Method for Plane-Strain Fracture Toughness of Metallic Materials, (ASTM E 399-90), American Society for Testing and Materials, West Conshohocken, PA, 1995.
- [43] J.R. Rice, M.A. Johnson, The role of large crack tip geometry changes in plane strain fracture, in: M.F. Kanninen, W.F. Adler, A.R. Rosenfield, R.I. Jaffee (Eds.), *Inelastic Behavior of Solids*, McGraw-Hill, New York, NY, 1970, p. 641.
- [44] J.K. Shang, R.O. Ritchie, *Met. Trans.* 20A (1989) 897.
- [45] A. Mortensen, Fabrication of Particulates Reinforced Metal Composites: Proceedings of an International Conference, Montréal, Québec, Canada, 17–24 September, 1990, ASM International, Materials Park, OH, 1990, p. 217.
- [46] B. Maruyama, Method for Making Metal Matrix Composites, US Patent Number 6,033,622 (March 7, 2000).
- [47] A.J. Sherman, R.H. Tuffias, *Ceramic Eng. Sci. Proc.* 11 (1990) 1500.
- [48] G.M. Chow, L.K. Kurihara, L.J. Martinez-Miranda, *Appl. Phys. Lett.* 70 (1997) 2315.
- [49] T.N. Baker, A.J. Gorton, H. Carvalhinhos, *Powder Metall.* 39 (1996) 223.
- [50] A. Mortensen, V.J. Michaud, M.C. Flemings, *JOM* 45 (1993) 36.